ARTICLE | Article in Press

Subsurface basin structure, seismic site conditions and earthquake damage: case study of the Gölbaşi basin, Türkiye

Aydın Büyüksaraç · Özcan Bektaş · Eren Pamuk · Seyhan Fırat · Ercan Işık · Nihat Sinan Işık · Kemal Önder Çetin

Received: 11 May 2026 / Accepted: 28 September 2026
© The Author(s) 2026

Abstract

Gölbaşı (Adıyaman) Town, located within a basin along a left-stepping segment of the East Anatolian Fault Zone in Türkiye, experienced severe damage during the 6 February 2023 Mw 7.8 and Mw 7.6 Kahramanmaraş earthquakes. Widespread liquefaction, ground subsidence, lateral spreading, bearing capacity failures and building collapses occurred, with their spatial distribution suggesting a strong association between basin geometry and ground motion amplification. This study investigates the subsurface geometry and sediment thickness of the Gölbaşı Basin using an integrated approach combining microgravity measurements and Spatial Autocorrelation (SPAC) analyses. A total of 120 microgravity measurements were conducted to delineate the lateral and vertical extent of low-density alluvial deposits, and two-dimensional gravity models were constructed along four profiles. Additionally, SPAC measurements at 20 locations yielded deep shear-wave velocity (Vs) profiles, from which Vs30 values were derived. Basin-depth proxies ($Z_{1.0}$ and $Z_{2.5}$) were subsequently estimated from Vs30 using empirical relationships. The basin contains up to approximately 700 m of unconsolidated sediments. Variations in sediment thickness and basin geometry produce significant lateral heterogeneity in seismic velocity and impedance contrasts across the basin. Areas underlain by the thickest sediments experienced the most severe structural damage. The results demonstrate a strong spatial association between sediment thickness, basin geometry, seismic site conditions, and the observed distribution of structural damage. A neighborhood-based Pearson correlation analysis revealed a very strong positive relationship between the severe-damage ratio and sediment thickness ($r=0.905$, $p<0.001$), a strong positive correlation with $Z_{2.5}$ ($r=0.763$, $p=0.017$) and a strong negative correlation with Vs30 ($r=-0.698$, $p=0.037$). Although the correlations with $Z_{1.0}$ and the gravity anomaly did not reach the 5% significance level, they exhibited similarly strong spatial trends. Given the limited number of neighborhoods analyzed ($n=9$), these results are interpreted as exploratory spatial associations rather than evidence of causal relationships. Nevertheless, the agreement among the gravity-derived basin geometry, SPAC-derived site parameters, and the damage analysis indicates that sediment thickness and subsurface basin structure were significant contributors to the spatial distribution of earthquake damage.

This Article in Press is shared early to give you faster access to new research. It is citable and carries a permanent DOI. The final edited version will replace it automatically.

https://doi.org/10.1038/s41598-026-74086-2

Published online: 01 October 2026

scientific reports

Keywords Basin effects · Ground motion amplification · Local site effects · Microgravity · SPAC · Shear-wave velocity · Earthquake damage

Introduction

The impact of local soil conditions on earthquake motion is a critical research area for seismic hazard assessment and earthquake engineering. The characteristics of earthquake ground motion, including its amplitude, frequency content, and duration, are controlled by earthquake source properties, wave propagation effects, and local site conditions. These processes have long been recognized as one of the primary causes of spatial variability in earthquake damage[1–4]. Because direct site response analyses are rarely available over large regions, the time-averaged shear-wave velocity of the upper 30 m (Vs30) has become the most widely used proxy for site classification in seismic design codes and ground-motion prediction equations[2,5,6]. However, numerous observational and numerical studies have demonstrated that Vs30 alone cannot adequately represent site response in deep sedimentary basins, where basin geometry, sediment thickness, impedance contrasts and three-dimensional wave propagation significantly influence earthquake ground motions[4,7–10]. Consequently, additional proxies such as $Z_{1.0}$ and $Z_{2.5}$ have been incorporated into modern ground-motion prediction models to better represent deep basin effects[5,11].

While conventional one-dimensional site response models explain amplification through the resonance of soft soil layers overlying stiff bedrock, observations from large sedimentary basins demonstrate that these simplified models cannot fully capture basin-induced effects. Complex basin geometries generate two- and three-dimensional wave propagation phenomena, including basin-edge diffraction, wave trapping, and surface-wave generation, which significantly modify both the amplitude and frequency content of ground motions[1,9,12]. These processes often explain spatial variations in earthquake damage that cannot be attributed solely to shallow soil conditions.

Integrated geophysical investigations combining microgravity surveys with Spatial Autocorrelation (SPAC) measurements provide an effective approach for reconstructing deep basin geometry and subsurface velocity structures relevant to seismic site response. Previous studies have successfully applied these methods to sedimentary basins such as Adapazarı, İzmit, Leonessa, İzmir, and Çanakkale, demonstrating their capability to estimate sediment thickness, engineering bedrock depth, and basin architecture for seismic microzonation and hazard assessment[13–19]. Recent post-earthquake investigations in sedimentary basins have further emphasized the importance of integrated geophysical approaches for evaluating basin-controlled site effects. In the Oued Martil floodplain (Northern Morocco), microtremor-based investigations demonstrated that thick fluvial sediments significantly modified local seismic response through impedance contrasts and basin geometry[20]. Similarly, following the 2023 Al Haouz earthquake, integrated geophysical analyses of the High Atlas sedimentary basin showed that variations in sediment thickness and subsurface velocity structure exerted a strong influence on site amplification and seismic hazard characterization[21]. These studies further demonstrate that deep sedimentary basin geometry should be considered together with shallow site conditions when assessing earthquake ground motion and seismic risk.

Following the devastating 6 February 2023 Kahramanmaraş earthquake sequence (Mw 7.8 and Mw 7.6), numerous studies investigated structural damage, liquefaction, foundation failures, and post-earthquake geotechnical conditions in Gölbaşı and Antakya. These studies clearly demonstrated the importance of local ground conditions in controlling earthquake damage. Nevertheless, the influence of deep basin geometry on the observed damage distribution has not yet been quantitatively evaluated using integrated geophysical datasets.

This study addresses this knowledge gap by integrating microgravity measurements with SPAC-derived shear-wave velocity models to characterize the three-dimensional geometry and sediment thickness of the Gölbaşı Basin (Fig. 1). Basin-depth parameters (Vs30, $Z_{1.0}$, and $Z_{2.5}$) are evaluated together with gravity-derived basin geometry to investigate the role of deep sedimentary structure in controlling seismic site amplification and the

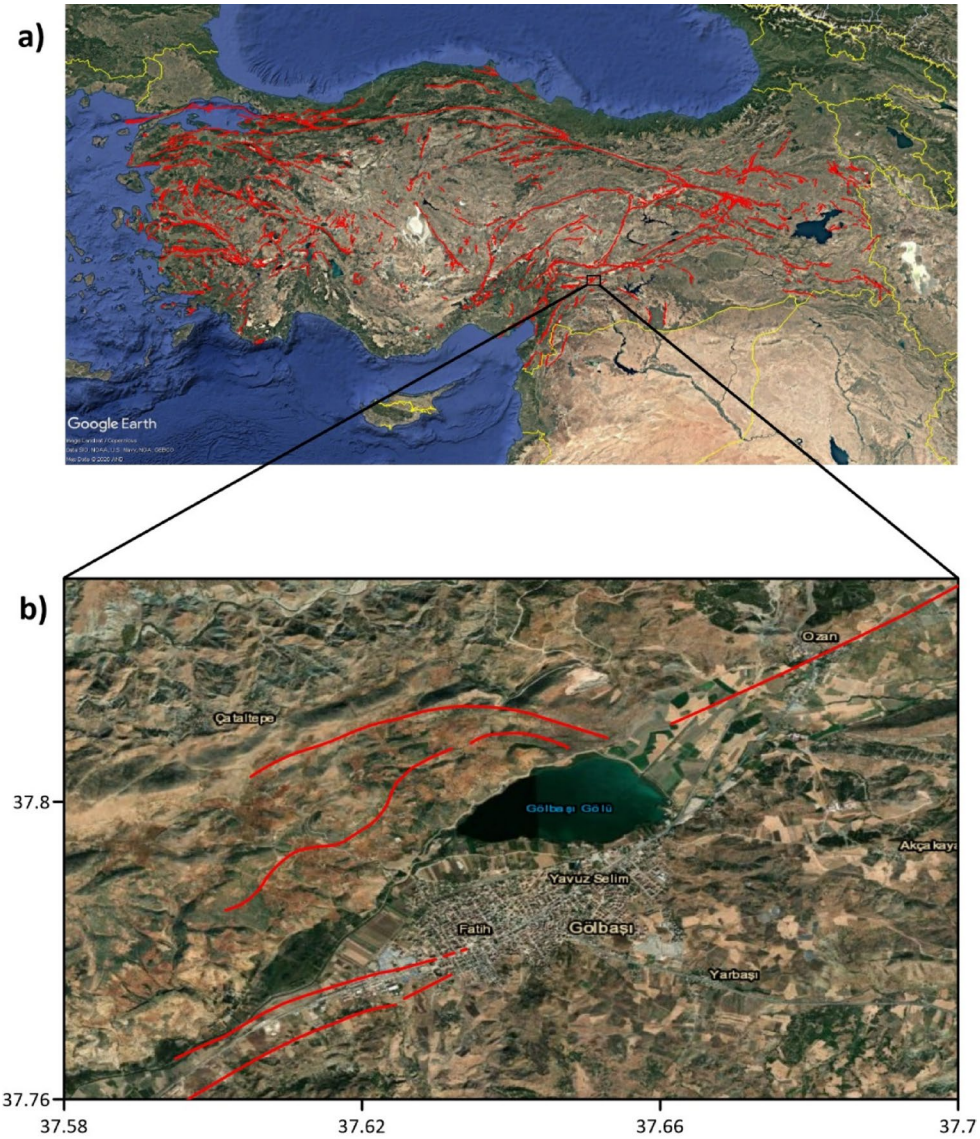


Fig. 1 **(a)** The regional tectonic setting of Türkiye and the location of the study area shown as black rectangular. **(b)** Google Earth satellite image of the Gölbaşı Basin and surrounding area (Adıyaman, Türkiye). Red lines indicate active fault zones within the study area (obtained from[22].

spatial distribution of earthquake damage. Unlike previous post-earthquake investigations that primarily focused on liquefaction, structural performance, and reconnaissance observations, the present study provides a quantitative assessment of deep basin effects and demonstrates that deep subsurface conditions explain the observed damage distribution more effectively than shallow site parameters alone.

Geological setting and earthquake damage distribution in Gölbaşı basin

Regional tectonic setting

The Eastern Anatolian Fault System (EAFS) makes a left-lateral step-over around the Gölbaşı area, splitting into two different fault segments. These are the Erkenek and Pazarcık Segments, which control the NE and SW margins of the basin, respectively. The Gölbaşı Basin, developed under the control of these two segments, is a pull-apart basin formed within the EAFS (Fig. 2). Within the basin, the Pazarcık Segment splits into two branches.

During the February 6 earthquakes, surface ruptures developed along both traces, but the most prominent ones occurred on the northern branch. Therefore, this branch has been interpreted as the main strand of the Pazarcık Segment.

The northeastern continuation of the Gölbaşı–Türkoğlu segment is partially covered by alluvial fans and lake deposits. Therefore, the trace of the active fault around Gölbaşı is unclear. Although there is a linear NE–SW-trending morphological scarp to the northeast of Lake Gölbaşı, no evidence of active faulting has been observed along this scarp. Considering that the distance between the two segments is approximately 800 m, it is unlikely that such a step-over would produce a basin longer than 25 km and up to 3 km wide.

Instrumental earthquakes (Mw≥3.0) and historical earthquakes affecting Gölbaşı and its surroundings are presented in Fig. 3. In the figure, the epicenters of the 6 February 2023 Kahramanmaraş earthquakes (Mw 7.8 and Mw 7.6) have also been included, and the location of the Gölbaşı Basin has been clearly indicated. The distribution of seismicity shows that earthquakes are concentrated mainly to the north and east of Gölbaşı, particularly in the region bounded by the Çardak Segment of the East Anatolian Fault Zone, the Adıyaman Fault Zone, and the Pazarcık Segment. The figure provides a clearer illustration of the regional seismotectonic setting of the study area and highlights the relationship between the Gölbaşı Basin and the major active fault systems responsible for the 2023 earthquake sequence.

Basin evolution and structural characteristics

The Gölbaşı Basin cannot be considered a classical pull-apart basin. The Erkenek and Pazarcık segments of the EAFS losing their continuity by stepping leftward to the northeast and southwest of the Gölbaşı Basin, can be listed as the strongest evidence that the Gölbaşı Basin was developed as a pull-apart basin associated with a fault step-over. Moreover, although these two fault segments displaced together during the February 6 earthquakes, they did not link up, providing the most significant evidence that the pull-apart process is still ongoing.

The Gölbaşı basin, located between the northeastern end of the Gölbaşı–Türkoğlu segment and the southwestern end of the Çelikhan–Erkenek segments of the East Anatolian Fault Zone (EAFZ), is a 1.5–7 km wide, 35 km

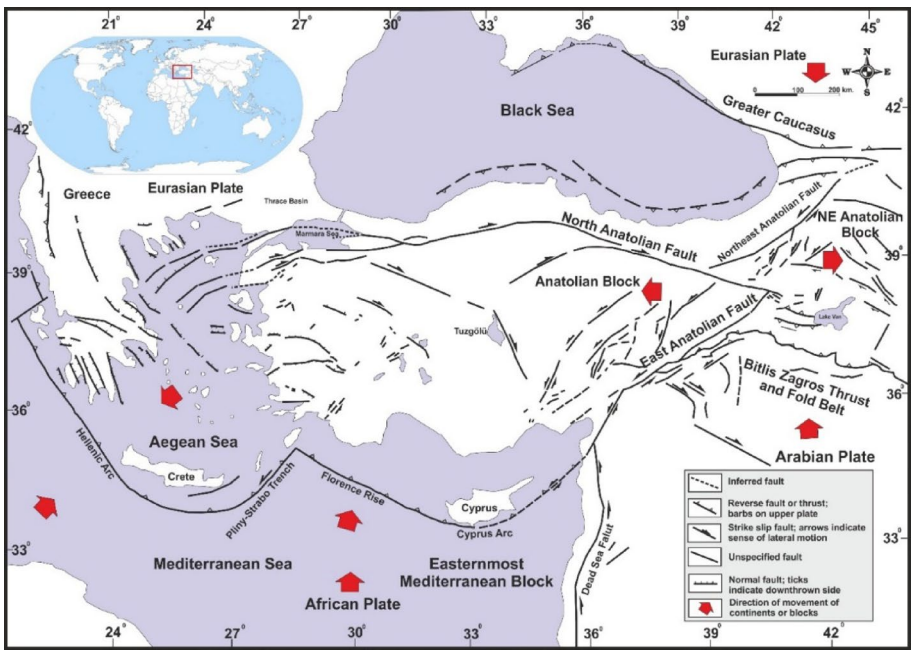


Fig. 2 Locations of active tectonic elements in Anatolia and its surroundings.(modified from)[23–26].

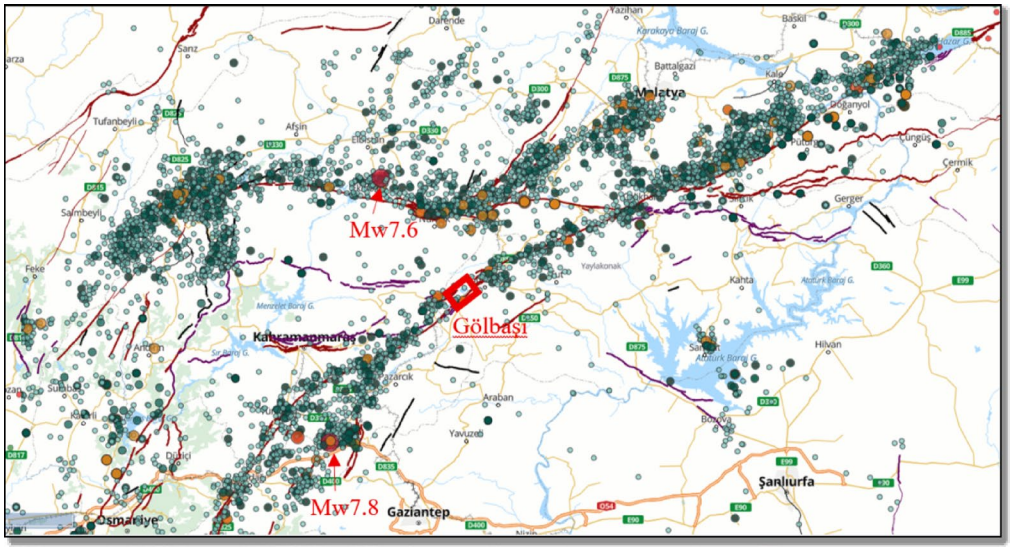


Fig. 3 Regional seismotectonic map of the Gölbaşı Basin showing instrumental earthquakes (Mw≥3.0), historical earthquakes, the epicenters of the 6 February 2023 Kahramanmaraş earthquakes (Mw 7.8 and Mw 7.6), major active faults, and the location of the Gölbaşı Basin.

long, N-NE axis strike-slip faulting basin. The basin narrows and ends at the northeastern and southwestern ends, while it reaches a width of approximately 7 km at the center.

Basin stratigraphy

The basin deposits consist of various sedimentary facies and basalt flows that are laterally and vertically transitional. The facies other than the basalt flow are divided into two groups according to grain size and depositional environment: (1) coarse-grained marginal facies and (2) fine-grained basin mid-facies. The marginal facies are mainly represented by fault terrace conglomerates, fan-apron sediments and fan-delta sediments. The first and oldest unit of the basin, the terrace sediments, consist of semi-consolidated, variously layered, mostly unsorted, multi-component conglomerate, sandstone and mudstone alternations. These first sediments of the basin have been partially deformed by the faults, which also controlled their depositional characteristics. Simply put, they have been compressed to form pressure ridges or uplifted to form fault-bounded terraces at different elevations relative to the surrounding bedrock. Sometimes, they have steepened up to 90º adjacent to the faults. These units were previously dated as Pliocene-Quaternary and named as Pazarcık Formation[27]. The fact that these units were also cut by basalt flows of 1.3–1.5 Ma confirms the age. These consist of fan sediments deposited by streams flowing into the basin, along the basin margin faults and under their control, and slope deposits accumulated under the effect of gravity along the fault scarp and foothills.

The sedimentary succession formed by the gradual merging of these two facies and extending across both margins of the basin represents the fan-apron facies. In general, the fan-apron facies determine the short periods when the faults are inactive, while the young fans developing on them determine the periods when the faults are active. The coarse-grained margin facies contain many faults of different sizes that are as old as sedimentation and younger. The second important facies of the basin fill are the finer-grained sand, silt and organic-rich muds deposited in the middle of the basin. Fine-grained facies are vertically and laterally transitional with the coarse-grained margin facies. Except in the vicinity of the marginal faults and pressure ridges, the Gölbaşı Basin deposits are generally undeformed and remain nearly horizontal. They unconformably overlie the folded Late Miocene–Early Pliocene units across an angular unconformity, locally marked by thrust-fault contacts. This observation indicates that there was a significant change in the tectonic regime during the period after the deposition of the

Esmepuru and Döndükler formations[27], before the start of the Gölbaşı basin depositional process. These relationships indicate a major change in the regional tectonic regime prior to the initiation of basin sedimentation and demonstrate that sedimentation evolved synchronously with strike-slip deformation.

Earthquake damage distribution

Gölbaşı (Adıyaman) was among the settlements most severely affected by the 6 February 2023 Kahramanmaraş earthquake sequence (Mw 7.7 and Mw 7.6). The earthquakes caused extensive structural damage and widespread ground failures, including soil liquefaction, ground settlement, lateral spreading, bearing-capacity failures, and sand boils. Numerous residential buildings experienced excessive tilting, differential settlement, partial collapse, or total collapse, rendering many structures unusable. Although construction quality, structural design deficiencies, and non-compliance with seismic design principles undoubtedly played an important role in the observed damage[28–31], the thick lacustrine alluvial deposits underlying the Gölbaşı Basin significantly amplified these adverse effects. These observations motivated detailed post-earthquake investigations aimed at identifying the causes of damage and supporting future rehabilitation and reconstruction efforts. Within this framework, the present study employs integrated microgravity and Spatial Autocorrelation (SPAC) methods to determine basin geometry, alluvial thickness, and their implications for urban development and earthquake damage.

Historical development of the settlement also provides important context for understanding the earthquake damage. Until the construction of the railway along the southern shore of Lake Gölbaşı during the 1930 s, the district contained only limited settlements. Since the establishment of the modern town, no major earthquake had affected the area before the 2023 earthquake sequence. Consequently, neither the seismic performance of the existing building stock nor the suitability of constructing urban areas on thick lacustrine alluvial deposits had previously been tested under strong ground shaking.

Representative examples of structural and ground damage are presented in Fig. 4. Severe damage was concentrated particularly in areas characterized by weak soil conditions. Field observations indicate that structural deficiencies, including soft-storey mechanisms, torsional irregularities, inadequate reinforcement detailing, and other plan and vertical irregularities, acted together with unfavourable soil–structure interaction to increase damage severity. Brittle column failures, shear failures, soft-storey collapse mechanisms, and differential settlements caused by weak foundation soils were among the predominant damage patterns. These findings demonstrate that earthquake risk cannot be evaluated solely from seismic hazard, but must also incorporate local geological conditions, geotechnical characteristics, and structural vulnerability.

Following the earthquakes, numerous investigations examined damage in Gölbaşı from complementary disciplinary perspectives. Structural reconnaissance studies documented widespread collapse, tilting, settlement, and severe deficiencies in load-bearing systems[32–35]. Other studies emphasized that thick unconsolidated lacustrine sediments combined with the widespread use of shallow foundations substantially increased structural vulnerability[36]. Soil-related investigations consistently reported extensive liquefaction, cyclic softening, lateral spreading, widespread ground settlement, and bearing-capacity failures, particularly within the northeastern part of the Gölbaşı Basin along the East Anatolian Fault rupture[32,37–40]. These observations were supported by detailed post-earthquake reconnaissance, geotechnical investigations involving 91 boreholes, cyclic triaxial testing, and LiDAR surveys documenting perishable liquefaction features[41,42].

Additional studies further demonstrated that Gölbaşı experienced exceptionally strong ground shaking, with Peak Ground Acceleration (PGA) values approaching 1.0 g and Modified Mercalli Intensity (MMI) levels reaching IX, particularly in areas underlain by weak soils[44]. Provost[45], identified a previously unmapped fault trace west of the Gölbaşı releasing bend, improving the tectonic framework of the basin. Toprak[46], showed that many failures within the natural gas distribution network occurred where the East Anatolian Fault intersects the district center and Lake Gölbaşı Basin, emphasizing the combined influence of fault rupture, basin geometry, and critical infrastructure. Collectively, previous studies consistently indicate that severe damage in Gölbaşı resulted from



Fig. 4 Structural damage caused by soil conditions in the study area[43].

the combined effects of basin-controlled site amplification, widespread liquefaction, differential settlement, surface faulting, and structural deficiencies.

Official post-earthquake damage assessments conducted by the Ministry of Environment, Urbanization and Climate Change classified buildings as undamaged, slightly damaged, moderately damaged, heavily damaged, requiring urgent demolition, or collapsed. According to these assessments, 6,872 buildings were evaluated within the study area, of which 169 (2.5%) were classified as collapsed, 1,592 (23.2%) as heavily damaged or requiring urgent demolition, 636 (9.3%) as moderately damaged, and 2,765 (40.2%) as undamaged.

The characteristics of the investigated building stock further explain the observed damage pattern. Approximately 74% of the buildings were reinforced concrete structures, 26% were masonry buildings, and nearly 70% had been constructed before 2000, prior to the implementation of modern Turkish seismic design regulations.

Most buildings consisted of one to two stories (63%), three to four stories (27%) and were commonly founded on shallow foundations resting on loose, water-saturated lacustrine sediments.

Geophysical methods

Spatial autocorrelation (SPAC) method

Determining the deep subsurface structure in settlement areas that exhibit basin characteristics is critically important for ensuring safe habitation during earthquakes. For this reason, it is necessary to obtain bedrock or the engineering bedrock depths. Additionally, due to the site effects observed in basins during earthquakes, leading to much higher amplitudes than those expected at site at similar distances from the fault rupture. To assess these site effects, Vs profiles need to be developed. SPAC measurements are used for this purpose. Previous studies have successfully identified resonance frequencies, assessed seismic site response, and delineated basin structures in regions such as Van, Bursa, and northwestern Türkiye[47–49]. These studies demonstrate the reliability and effectiveness of microtremor-based approaches for seismic microzonation and earthquake hazard assessment. They were conducted at 20 locations covering the Gölbaşı Basin to obtain deep Vs values. Pamuk[50], evaluated the SPAC data obtained and produced Vs30 and $Z_{0.76}$ distribution maps. However, impedance contrasts triggering more pronounced local site effects can occur at depths greater than the upper 30 m, which undermines the effectiveness of Vs30 as a proxy for site effects ([5]. Notably, $Z_{2.5}$ can also be interpreted as the depth to seismic bedrock or the reference rock. In basins, if $Z_{2.5} > 3$ km, a three-dimensional basin effect is present, whereas if $Z_{2.5} < 1$ km, a shallow sediment effect dominates. In the case of shallow sediments—meaning small $Z_{2.5}$ values—if Vs30 is also low, resonance is expected to occur, influencing the velocity-band behavior of earthquake ground-motion spectra and increasing the period in acceleration spectra ([5]. Therefore, $Z_{1.0}$ and $Z_{2.5}$ values are also other useful proxies that must be considered to accurately assess local site effects.

Data acquisition and processing

Circular-array microtremor measurements based on the Spatial Autocorrelation (SPAC) method were conducted to estimate the deep one-dimensional shear-wave velocity (Vs) structure beneath the Gölbaşı Basin. The SPAC method derives the phase-velocity dispersion curve of Rayleigh waves from ambient seismic noise recorded by a circular sensor array. These dispersion curves are subsequently inverted to obtain one-dimensional Vs–depth profiles using inversion algorithms. Each SPAC array consisted of a central station surrounded by three or four peripheral stations arranged on a circle. To investigate progressively greater depths, measurements were performed using three or four array diameters at each site. A total of 20 measurement locations were distributed across the basin to characterize the lateral variability of the subsurface structure. Only the vertical components of the three-component microtremor recordings were used for SPAC analysis. The vertical-component records from all sensors within each circular array were processed simultaneously using Geopsy software to calculate the Rayleigh-wave phase velocity dispersion curve, which was assigned to the center of the array. Subsequently, inversion of the dispersion curve was performed to obtain a one-dimensional shear-wave velocity (Vs) profile, representing the variation of Vs with depth beneath each measurement location. The array configuration employed in the Gölbaşı Basin, together with representative vertical-component (Z-component) microtremor records from four measurement sites, is shown in Fig. 5. Ambient-noise data were acquired using SMART-SOLO IGU-BD3C-5 three-component seismometers using internal GPS timing system with a natural frequency of 0.2 Hz and a sampling interval of 0.25 ms. At each measurement location, microtremor signals were continuously recorded for 60 min, providing sufficient data quality for reliable estimation of the Rayleigh-wave dispersion curves and subsequent inversion.

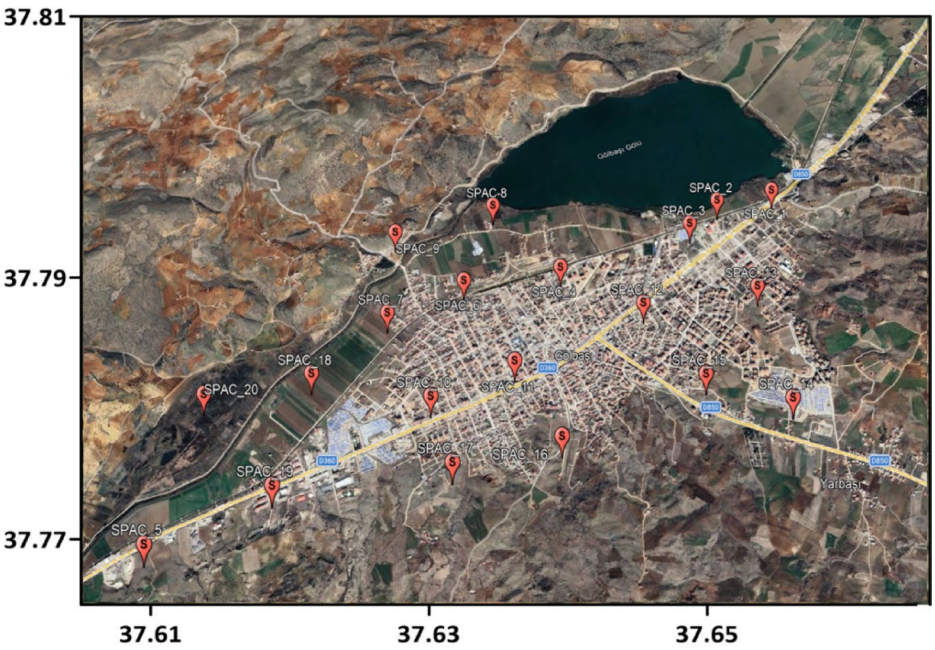


Fig. 5 Distribution of the 20 Spatial Autocorrelation (SPAC) measurement sites superimposed on a satellite image of the Gölbaşı (Adıyaman) Basin. The numbered stations (SPAC-1 to SPAC-20) represent the locations where ambient-noise measurements were acquired for the SPAC analysis.

Basin-depth parameters

In the study, by using the Vs30 values from SPAC measurements along with Eqs. 1 and 2 proposed by Chiou and Youngs[11], the $Z_{1.0}$ and $Z_{2.5}$ contour maps were generated as shown in Fig. 6.

$$Z_{1.0} = Exp[28.5 - \frac{3.82}{8}\ln\left(Vs_{30}^{8} + 378.7^{8}\right)] \quad (1)$$

$$Z_{2.5} = 519 + 3.595Z_{1.0} \quad (2)$$

Here, Vs30 represents the time-averaged shear-wave velocity within the upper 30 m of the subsurface and is expressed in m/s. $Z_{1.0}$ denotes the depth (in m) to the horizon where the shear-wave velocity first reaches 1.0 km/s, whereas $Z_{2.5}$ represents the depth (in m) to the horizon where the shear-wave velocity reaches 2.5 km/s.

The empirical relationships proposed by Chiou and Youngs[11] were originally developed using the NGA-West1 database, which mainly represents tectonically active regions of western North America. Although these equations have been widely adopted in ground-motion prediction studies for estimating basin-depth parameters ($Z_{1.0}$ and $Z_{2.5}$) from Vs30, their direct applicability to the geological conditions of the Gölbaşı Basin has not been specifically validated. Therefore, in this study, the Vs30-based empirically estimated $Z_{1.0}$ and $Z_{2.5}$ values are interpreted as first-order proxies describing the relative spatial variation of basin depth and impedance contrasts rather than exact measurements of engineering bedrock depth. Consistent with the gravity results, the central basin is characterized by relatively low Vs30 values of approximately 280–350 m/s, indicating soft soil conditions, whereas the basin margins generally exhibit Vs30 values exceeding 550 m/s, corresponding to stiffer geological units. Similarly, the estimated $Z_{2.5}$ values exceed 1300 m in the central basin and decrease to approximately 1000 m towards the basin margins, reflecting the progressive shallowing of the seismic bedrock.

Microgravity measurements

The gravity method was most used in oil and gas exploration, especially in the early twentieth century. However, practice suggested that the method can be used very widely in mapping the thickness of unconsolidated beds where ground motion amplification can occur. The gravity field is the gravitational force applied to a unit mass

https://doi.org/10.1038/s41598-026-74086-2

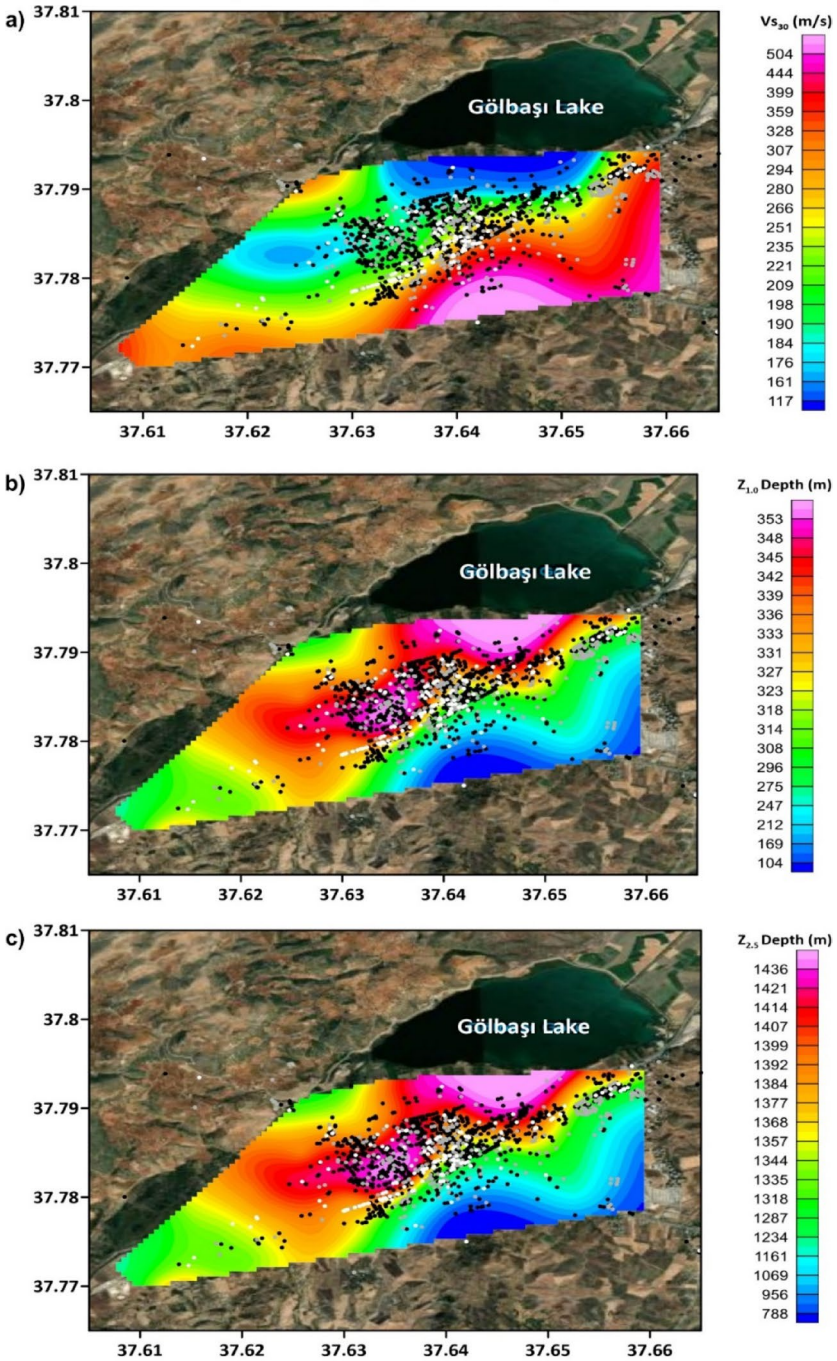


Fig. 6 **(a)** Vs30 distribution for the Gölbaşı district, **(b)** Depth distribution at which 1.0 km/s Vs velocity is reached ($Z_{1.0}$) and **(c)** Depth distribution at which 2.5 km/s Vs velocity is reached ($Z_{2.5}$). White squares indicate collapsed buildings, black squares indicate heavily damaged buildings, and gray squares indicate moderately damaged buildings.

at a point on or near the earth's surface in space. Gravity is also a geophysical potential field method. Recently, it has been frequently used especially for loose layer/bedrock modelling of cities with basin settlements. The gravity method can also detect geological differences and contacts (faults) using density gradient interpretation techniques. It is mainly dependent on the differences in the density of the ground layers. Variations in the underground rock density led to changes in the observed gravity field.

Data acquisition and processing

A microgravity study covering the entire basin was conducted to determine the lateral and vertical boundaries of the Gölbaşı Basin. With this study, it was possible to distinguish between the low-density sediment part of the basin and the bedrock. In the measurements made in the study area, microgravity values were obtained at a total of 120 points with a sampling interval of 400 × 400 m as shown in Fig. 7. The study area covers densely populated areas and partially vacant lands. During the measurement, four base points were determined and then these points were combined at a reference point at the midpoint of the area. During the measurement, three readings were taken at each measurement point and the average of these readings was taken and recorded. Microgravity data were collected with the Scintrex CG-5 Autograv device, and Leica RX 1250XC and Leica GPS 1200 + equipment sets were used for height and positioning measurements. The corrected gravity values were subsequently converted into Bouguer gravity anomalies using the standard gravity reduction procedure (Eq. 3), and residual anomalies were obtained after removing the regional trend by polynomial fitting.

$$\Delta g_B = (g_{obs} - g_{base}) + C_{drift} + C_{Lat} + C_{FA} - C_B \quad (3)$$

here,

$\mathbf{\Delta g_{i:}}$ Gravity difference (or residual gravity value) at observation station **i** (mGal).

$\mathbf{g_{i:}}$ Observed gravity value at observation station **i** before corrections (mGal).

$\mathbf{g_{base:}}$: Gravity value measured at the base (reference) station (mGal).

$\mathbf{C_{drift:}}$ Instrument drift correction, applied to compensate for temporal variations in the gravimeter response during the survey (mGal).

$\mathbf{c}_{LAT}$: Latitude correction, which removes the effect of the Earth's ellipsoidal shape and rotation on gravity (mGal).

$\mathbf{c}_{FA}$: Free-air correction, applied to compensate for the elevation of the measurement point above the reference datum (mGal).

$\mathbf{c}_{B}$: Bouguer slab correction, which removes the gravitational attraction of the rock mass between the measurement point and sea level, assuming an infinite horizontal slab of constant density (mGal).

Regional effect makes it difficult to process gravity data with potential field data evaluation method. Therefore, it is necessary to obtain residual anomaly data by eliminating the regional effect in the data. One of the techniques used in the separation of regional-residual anomalies is trend analysis. This analysis is done with linear, orthogonal, etc. polynomials. The process of determining the general trends of underground structures at a regional scale is called trend analysis. For this, the relationship coefficient between the measured data and the data calculated

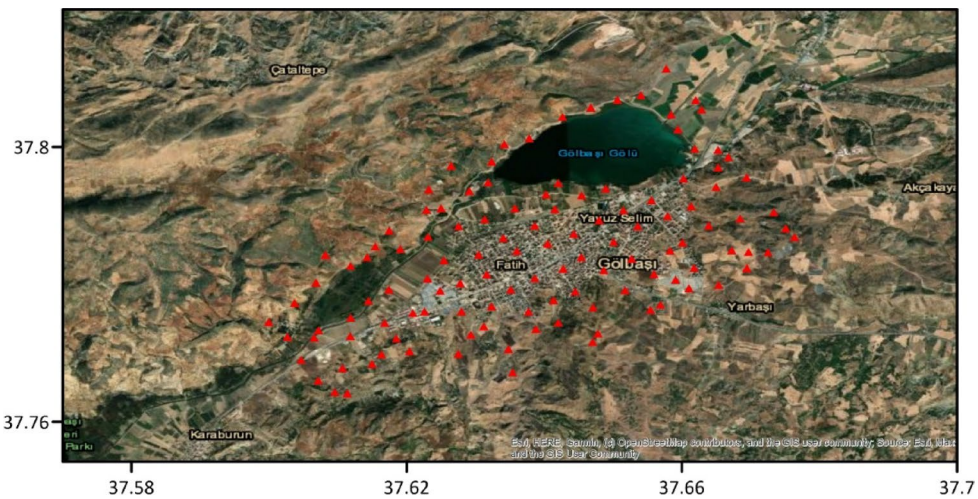


Fig. 7 Distribution of microgravity measurement points in the Gölbaşı (Adıyaman) Basin. Red triangles represent microgravity stations acquired on a 400 m × 400 m grid.

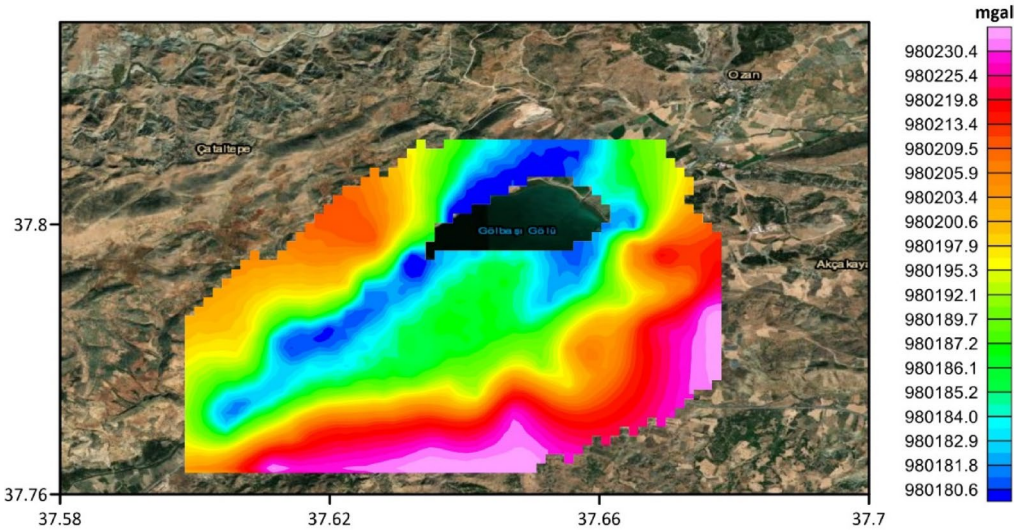


Fig. 8 Bouguer gravity anomaly map of the study area.

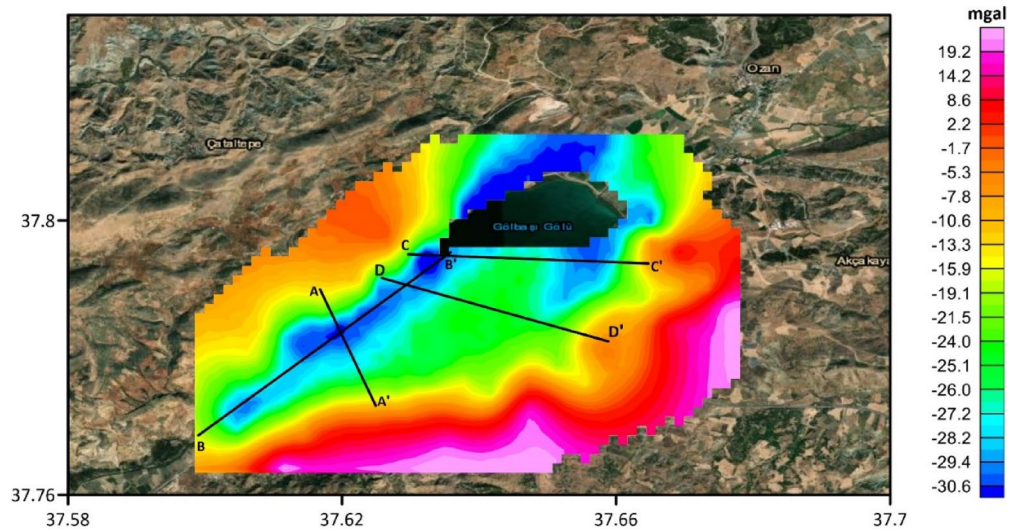


Fig. 9 Trend removed (residual) gravity anomalies of the study area. Layout of the four 2D gravity modeling profiles across the Gölbaşı Basin (Adıyaman, Türkiye). The profiles, oriented in different directions, were used to investigate subsurface density variations and basin geometry.

with polynomials is calculated. In this calculation, the degree of the polynomial with the highest curvature of the parabola is taken as the trend degree, that is, the degree of the polynomial that will give the regional anomaly. The data of the regional anomaly calculated with this degree is subtracted from the measured data and the residual anomaly data is calculated. Regional and residual gravity anomalies were separated using polynomial trend analysis. Several polynomial orders were examined, and the final trend surface was selected based on the best agreement between the calculated regional field and the long-wavelength gravity variations while preserving the short-wavelength anomalies associated with basin-scale structures. In this study, the regional trend of the Bouguer gravity anomaly (Fig. 8) was represented by a second-order polynomial trend surface, and residual gravity anomalies were obtained by subtracting this trend from the observed data. The resulting residual gravity anomalies are shown in Fig. 9. The two-dimensional gravity models were constructed according to the criteria proposed by Nettleton (1940)[51].

There are various methods for calculating the gravity effect created by irregularly shaped two-dimensional structures. These methods are divided into two categories. The first method includes mesh, point representation and some calculation aids. However, the application of these methods is difficult and time-consuming in practice.

The second method is to divide irregular structures into simple geometric shapes and calculate the gravity effect more easily. The structure is divided into rectangular blocks, as suggested by Vening Meinesz[52]. However, the large number of blocks makes calculations difficult. At the same time, since the reduction of block sizes may cause the calculation of neglected values at distant points, it may increase the error rate in calculations. An irregular two-dimensional structure can be easily approximated to a closed polygon by keeping the number of edges high. The horizontal and vertical components of gravity at any given point can be calculated by analytical methods thanks to this polygon. There is no limitation on the size and location of the structure in the method. The important thing is to be able to draw a polygon that fully adapts to the structure and to increase the number of edges of the polygon as necessary. In order to create 2-dimensional gravity models from the residual gravity anomalies obtained as a result of microgravity measurements performed at 120 points, sections were taken along 4 profiles from the gravity anomaly map in Fig. 9. Two-dimensional gravity models were constructed along the profiles denoted as P1, P2, P3, and P4 in Fig. 10, and the resulting models are presented in Fig. 10. The SPAC measurement locations intersecting each profile were incorporated into the modelling, and the depth estimates derived from the SPAC analyses are also shown on the profiles. Accordingly, the two-dimensional gravity models were constrained and validated using the independent depth information obtained from the SPAC measurements.

The density values used in the 2D gravity models were selected based on the geological characteristics of the Gölbaşı Basin. The basin fill consists mainly of unconsolidated to weakly consolidated lacustrine and alluvial deposits, including clay, silt, sand, gravel, and organic-rich fine-grained sediments. Therefore, an average density of 1.6 g/cm³ was assigned to the sedimentary cover. In contrast, the underlying basement was represented by a density of 2.72 g/cm³, corresponding to relatively compact and older bedrock units surrounding and underlying the basin. These values were used as representative average densities to define the contrast between the low-density basin fill and the higher-density basement in the gravity modelling. Although local lithological variations may occur, the adopted density contrast is consistent with the geological setting of the study area and provides a reasonable first-order approximation for modelling the basin geometry. Although moderate variations in the assumed density contrast would affect the absolute sediment thickness estimates, the overall basin geometry, including the location of the principal depocenters and basin margins, remains robust. In addition, the gravity models were constrained by independent SPAC-derived shear-wave velocity information along the model profiles. The agreement between the gravity-derived sediment thicknesses and the SPAC-derived subsurface structure substantially reduces the ambiguity commonly associated with gravity interpretation and increases confidence in the inferred basin geometry. The dashed lines in the sections show the discontinuity boundaries (possible faults) of the sediments settled unconformably on the inferred bedrock. However, since there are no surface faulting traces supporting these discontinuities, there is no possibility of direct correlation.

It should be noted that gravity inversion is inherently a non-unique problem, since different combinations of subsurface geometry and density contrast may produce similar gravity anomalies. Consequently, the two-dimensional gravity models presented in this study should not be interpreted as unique solutions but rather as geologically constrained representations of the basin structure. To reduce this ambiguity, the modelling incorporated available geological information, including the distribution of unconsolidated basin-fill sediments and surrounding basement rocks, together with representative density values for each lithological unit. Furthermore, the gravity-derived basin geometry was independently evaluated using SPAC-derived shear-wave velocity profiles and basin-depth proxies, which provide complementary constraints on the subsurface structure. The consistency between the gravity models, the SPAC results, and the observed geological setting increases confidence in the interpreted basin geometry, although some uncertainty associated with gravity inversion inevitably remains. The Bouguer gravity anomaly map shows a clear spatial variation across the basin. The central part of the basin is characterized by relatively low gravity anomaly values ranging between approximately −16 and −18 mGal, indicating the presence of thick low-density sedimentary deposits. Towards the basin margins, gravity anomaly

https://doi.org/10.1038/s41598-026-74086-2

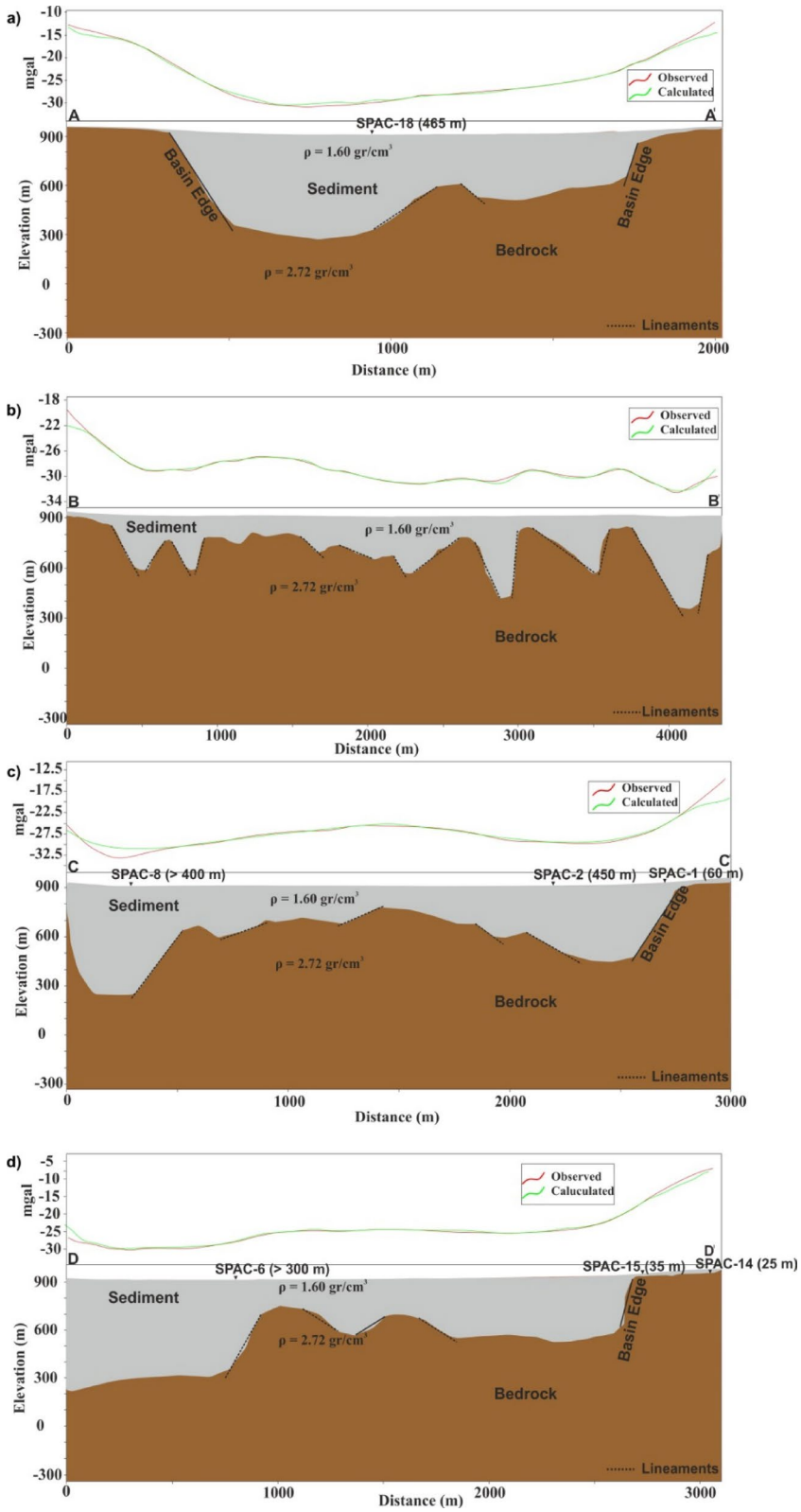


Fig. 10 Two-dimensional gravity models of the study area. The upper panels show the comparison between observed (red) and calculated (green) gravity anomalies, indicating a good fit with low RMS misfit values. The lower panels present the corresponding subsurface density models, where gray represents sedimentary deposits with a density of 1.6 g/cm³ and brown denotes basement rocks with a density of 2.72 g/cm³.

values gradually increase, reflecting shallower basement depths and thinner sedimentary cover. The calculated gravity responses closely match the observed anomalies, with RMS misfit values ranging from 0.12 to 0.24 mGal, indicating satisfactory model performance.

In the 2D A-A' gravity section of the P1 profile, 3 different sectors are observed. The deepest sediment with a thickness of 660 m was identified in the western section. Sediments of approximately 300 m and 400 m thick make the central and eastern sectors, respectively (Fig. 10a). In the 2D B-B' gravity section of the P2 profile, quite a "wavy" shape of the inferred bedrock top is observed. The deepest sector (west side) shows 700 m of sediments. The sediment bottom becomes relatively shallow (ca. 300 m deep) in the middle parts of the section. It becomes shallower towards the east of the section and deepens again to 300 m, eventually reaching a depth of 35 m on the basin edge (Fig. 10b). In the 2-dimensional C-C' gravity section of the P3 profile, very sudden and frequent sediment thickness changes are observed in the sediment bottom. A valley-like sedimentary geometry with a maximum sediment thickness of approximately 300 m is observed in the western part of the basin. In the central part, sediment thickness decreases to 10–250 m, whereas it increases again eastward, reaching depths of approximately 500–600 m (Fig. 10c). In the 2D D-D' gravity section (Profile P4), quite variable depths are observed of the sediment floor. The deepest part is the area with 700 m sediment thickness in the west. The sediment thickness becomes relatively shallow in the middle parts of the section, reaching depths of 200–250 m. Eastward, the sediments thicken again to 600–650 m becoming very thin (60 m) at the basin edge (Fig. 10d). In order to better pinpoint the structural boundaries and discontinuities in the study area, an edge-detector filter, in particular the Total Horizontal Derivative Filter (THD) was applied to the gravity anomalies shown in Fig. 10, as represented in Fig. 11. The filtered gravity data clearly enhance the basin boundaries and emphasize the lateral density contrasts between the sedimentary fill and the surrounding basement. Several local gravity lows become more distinct after filtering, indicating thicker sediment accumulation zones. In the same figure, the spatial distribution of building damage caused by February 6, 2023, earthquakes are superimposed on the interpreted basin geometry. The comparison reveals a clear spatial correspondence between the areas of severe damage and the thickest parts of the Gölbaşı Basin. In particular, the highest concentration of damaged buildings is observed where the sedimentary fill reaches its greatest thickness, suggesting a strong spatial association between deep basin geometry and the observed damage distribution. While other factors, such as building characteristics and

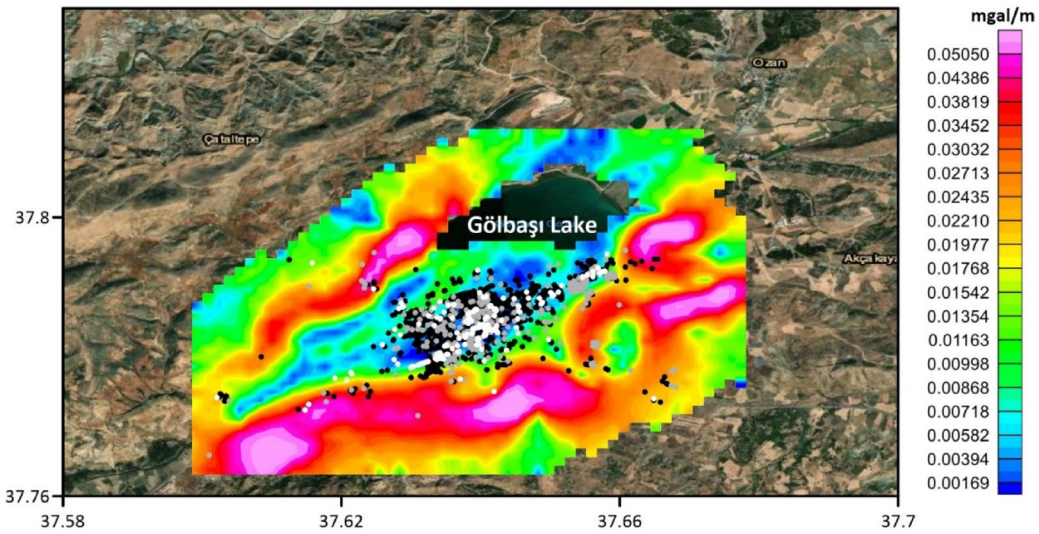


Fig. 11 Damage distribution from the February 6, 2023 earthquakes on the total horizontal derivative map resulting from the application of the THD filter to the Bouguer gravity anomalies. White squares indicate collapsed structures, black squares indicate heavily damaged structures, and gray squares indicate moderately damaged structures.

local geotechnical conditions, also contributed to the damage distribution, the observed spatial relationship highlights the importance of basin structure in the seismic response of the study area.

Results and discussion

Microgravity measurements reveal that the Gölbaşı Basin is characterized by a pronounced low-density sedimentary fill overlying a high-density bedrock. Residual gravity anomalies and two-dimensional models constructed along four profiles indicate that the thickness of unconsolidated alluvial deposits reaches up to approximately 650–700 m in the central and western parts of the basin. Toward the basin margins, the sediment thickness decreases sharply, reflecting a strong lateral heterogeneity of the basin geometry, controlled by faulting. In fact, the gravity-derived basin geometry shows a pronounced asymmetric structure, consistent with the pull-apart mechanism associated with the releasing bend (left-stepping geometry) between the Çelikhan–Erkenek and Gölbaşı–Türkoğlu segments of the East Anatolian Fault Zone[53,54]. The sudden changes in sediment thickness observed along several profiles suggest the presence of buried structural discontinuities and fault-controlled depocenters, even where surface fault traces are not evident. These geometric characteristics are typical of strike-slip basins[55,56] and have been widely recognized as factors that can influence seismic wave propagation and ground-motion amplification[57,58]. The gravity models are subject to uncertainties arising from the assumed density contrasts and the inherent non-uniqueness of gravity inversion. Although alternative density distributions may produce similar anomaly patterns, the overall basin geometry is constrained by regional geology, surface observations, and independent SPAC-derived velocity information. Consequently, while absolute basin depths may vary within a limited range, the interpreted spatial pattern of deep depocenters is considered robust.

SPAC analyses provided deep Vs profiles across the basin, enabling the estimation of Vs30 as well as depth parameters $Z_{1.0}$ and $Z_{2.5}$. A limitation of this study is that $Z_{1.0}$ and $Z_{2.5}$ were estimated using empirical equations derived from the NGA-West database rather than measured directly. Because basin sediment properties, depositional environments, and velocity gradients in the Gölbaşı Basin may differ from those represented in the original calibration dataset, the estimated depths are subject to uncertainty. Nevertheless, these parameters provide useful relative indicators of deep impedance contrasts and basin geometry, which are consistent with the independently derived gravity models.

The measurements exhibit generally low Vs30 values over the basin interior, indicating soft soil site conditions consistent with the lacustrine and alluvial nature of basin fill. However, the observed structural damage patterns cannot be solely attributed to variations in Vs30 values. Although Vs30 remains an effective proxy for near-surface site classification, its relatively limited spatial variability across the Gölbaşı Basin contrasts with the pronounced variations observed in $Z_{1.0}$ and $Z_{2.5}$. These deeper parameters exhibit a closer spatial correspondence with the gravity-derived basin geometry and the concentration of earthquake damage, suggesting that deep sedimentary structure exerts an additional control on site response beyond that represented by Vs30 alone. Vs30-based empirical estimated $Z_{1.0}$ and $Z_{2.5}$ values also increase significantly toward the central parts of the basin, where sediment thickness is greatest. In several locations, $Z_{1.0}$ exceeds a few hundred meters, indicating that impedance contrasts extend well below the shallow subsurface. The integration of microgravity-derived basin geometry with Vs-based parameters highlights the critical role of basin-induced ground motion amplification in Gölbaşı. Thick, low-velocity sediments overlying stiff bedrock may provide conditionsfavourable for resonance and seismic energy trapping within the basin. However, these mechanisms were not directly evaluated in the present study. In addition, the lateral heterogeneity of the basin enhances surface-wave generation and amplification, particularly at longer periods. The seismic bedrock depth ($Z_{2.5}$) varies approximately between 1000 and 1400 m. These values suggest that the Gölbaşı Basin does not belong to the class of extremely deep sedimentary basins where strong three-dimensional basin effects are generally expected to dominate. Nevertheless, the combination of thick unconsolidated sediments, pronounced lateral heterogeneity, and fault-controlled basin geometry, may have contributed to site conditions influencing the observed damage distribution, although the underlying mechanisms

were not directly evaluated in this study. Therefore, the observed damage distribution is interpreted as resulting from the combined influence of shallow site response and basin-controlled wave propagation, rather than from purely three-dimensional basin effects. These quantitative observations demonstrate that the deepest part of the basin, characterized by Bouguer gravity anomalies of −16 to −18 mGal, Vs30 values of 280–350 m/s, and $Z_{2.5}$ depths exceeding 1300 m, spatially corresponds to the area where earthquake damage was most concentrated. In contrast, the basin margins are characterized by relatively higher gravity anomaly values, Vs30 > 550 m/s, and shallower $Z_{2.5}$ depths of approximately 1000 m, indicating more competent subsurface conditions.

Previous studies have demonstrated that while pronounced three-dimensional basin resonance is generally associated with very deep sedimentary basins (> 3 km), shallower basins with sediment thicknesses of approximately 500–1500 m may still experience significant amplification due to resonance, basin-edge diffraction, wave focusing, and strong impedance contrasts between sediments and basement[1,4,9,12,14]. Considering the estimated sediment thickness (~ 700 m) and $Z_{2.5}$ depth (~ 1000–1400 m) of the Gölbaşı Basin, the observed spatial association is consistent with conditions that may favor relatively shallow basin-related amplification rather than from fully developed three-dimensional basin resonance. It is important to note that the gravity-derived sediment thickness and the estimated $Z_{2.5}$ parameter represent different physical interfaces within the subsurface. The gravity models delineate the boundary between the relatively low-density sedimentary fill and the denser basement rocks, whereas $Z_{2.5}$ is an empirical proxy representing the depth to the horizon where the shear-wave velocity reaches 2.5 km/s, estimated from Vs30-based empirical relationships. Therefore, the greater $Z_{2.5}$ depths (approximately 1000–1400 m) compared with the gravity-derived sediment thickness (~ 700 m) do not represent a contradiction. Rather, they reflect the different physical properties (density versus seismic velocity) and corresponding subsurface interfaces represented by these two parameters.

These results are consistent with previous studies demonstrating that two- and three-dimensional basin structures can significantly amplify ground motion relative to one-dimensional soil column models. The Gölbaşı Basin exhibits characteristics of a deep, laterally heterogeneous basin, where long-period amplification is expected to dominate, especially during large-magnitude earthquakes with rich low-frequency content, such as the Mw 7.8 and Mw 7.6 events. When the spatial distribution of earthquake damage is compared with the gravity and derivative maps, a clear correlation emerges between zones of severe damage and areas of maximum sediment thickness. Damage concentration is particularly evident in regions where gravity models indicate deep depocenters and where Vs30-based empirical estimates of $Z_{1.0}$ and $Z_{2.5}$ values are high. Conversely, areas near the basin margins, where bedrock is shallow and Vs values are higher, generally experienced less severe damage. This spatial correspondence suggests that basin geometry and sediment thickness exerted a first-order control on damage distribution, amplifying ground motions beyond what would be expected from shallow site conditions alone. While construction quality and building vulnerability undoubtedly contributed to the observed damage, the strong agreement between geophysical indicators and damage pattern emphasizes the dominant influence of local and basin-scale site effects. To further evaluate these spatial relationships quantitatively, a neighborhood-based statistical correlation analysis was performed between the severe building damage ratio and the geophysical parameters derived in this study.

To provide a quantitative assessment of the relationship between subsurface basin structure and building damage, the building inventory and damage data were aggregated at the neighbourhood level. The combined number of collapsed, immediately-to-be-demolished, and heavily damaged buildings was divided by the total building stock in each neighbourhood to calculate the severe-damage ratio. Neighbourhood-scale mean values of Vs30, $Z_{1.0}$, $Z_{2.5}$, gravity anomaly, and sediment thickness were then extracted from the corresponding maps. Pearson correlation coefficients were calculated between the severe-damage ratio and each geophysical parameter. Because the analysis included only nine neighbourhoods, the results were interpreted as exploratory spatial associations rather than direct evidence of causality (Table 1).

The neighbourhood-based analysis revealed a very strong positive correlation between the severe-damage ratio and sediment thickness ($r = 0.905$, $p < 0.001$), indicating that neighborhoods underlain by thicker sedimentary deposits experienced substantially higher levels of damage. Similarly, $Z_{2.5}$ exhibited a strong positive

Table 1 Pearson correlation analysis between neighborhood-based severe building damage ratio and the geophysical parameters derived for the Gölbaşı Basin.

Parameter	Pearson's *r*	*p*-value	Strength of Correlation	Statistical Significance ($\alpha = 0.05$)
Vs_{30}	−0,698	0.0365	Strong negative	Significant
$Z_{1.0}$	0,662	0.0520	Strong positive	Marginally significant
$Z_{2.5}$	0,763	0.0167	Strong positive	Significant
Gravity Anomaly	−0,643	0.0618	Strong negative	Not significant (borderline)
Sediment thickness	0,905	0.00079	Very strong positive	Highly significant

and statistically significant correlation ($r = 0.763$, $p = 0.017$), while Vs30 showed a strong negative correlation ($r = -0.698$, $p = 0.037$), suggesting that lower near-surface shear-wave velocities are associated with increased damage. Although $Z_{1.0}$ ($r = 0.662$, $p = 0.052$) and gravity anomaly ($r = -0.643$, $p = 0.062$) also displayed relatively strong correlations, these relationships did not reach the 5% significance level. Given the limited sample size ($n = 9$ neighborhoods), these results should be regarded as exploratory; nevertheless, they provide quantitative support for the observed spatial association between basin structure, seismic site conditions, and earthquake damage.

The findings obtained for the Gölbaşı Basin are consistent with observations from other tectonically active sedimentary basins worldwide. For example, ambient-noise and microtremor studies conducted in the Kashmir Basin (NW Himalaya) demonstrated that local seismic response is controlled not only by shallow site conditions but also by deep basin geometry, sediment thickness, and strong lateral velocity contrasts[59,60]. In addition, Gupta et al.[61], showed that the complex two- and three-dimensional basin architecture significantly influence wave propagation, resonance characteristics, and the spatial variability of seismic amplification. Similar to the Kashmir Basin, the Gölbaşı Basin exhibits a deep asymmetric sedimentary structure, where gravity-derived basin geometry and SPAC-derived velocity models indicate substantial lateral heterogeneity. The concentration of severe earthquake damage over the thickest sedimentary deposits suggests that basin-controlled amplification, together with local site conditions, plays a significant role in the observed damage distribution. These similarities indicate that the influence of deep sedimentary basin geometry on seismic ground motion is not unique to the Gölbaşı Basin but represents a common characteristic of tectonically active sedimentary basins.

The low Vs30 values indicate soft-site conditions that may have contributed to the observed structural damage. However, the underlying mechanisms, including possible resonance effects, were not directly evaluated in the present study. In regions like Gölbaşı, deep basin geometry and sediment thickness should be explicitly considered when evaluating seismic site conditions and earthquake damage patterns, particularly in sedimentary basins. The combined use of microgravity and SPAC methods provides an effective and relatively rapid approach for characterizing deep subsurface conditions relevant to earthquake engineering applications. These findings have important implications for seismic microzonation, urban planning, and risk mitigation strategies in Türkiye and other tectonically active regions with similar basin settings. Incorporating basin-scale effects into hazard assessments can lead to more realistic predictions of earthquake ground motion and, ultimately, to safer and more resilient urban development.

Although the present study demonstrates a clear spatial relationship between basin geometry, sediment thickness and the observed damage distribution, earthquake damage cannot be attributed solely to subsurface geological conditions. Building age, structural type, number of storeys, construction quality, foundation characteristics, liquefaction-induced ground deformation, and distance from the surface rupture also influenced the observed damage patterns. Previous post-earthquake investigations in Gölbaşı documented widespread liquefaction, differential settlement, shallow foundation problems and structural deficiencies, all of which contributed to building performance during the 2023 earthquake sequence. Therefore, the geophysical parameters evaluated in this study should be considered as one component of a multifactorial earthquake damage process rather than the sole controlling factor.

Conclusions

This study investigated the role of basin geometry and sediment thickness in controlling seismic site conditions and their spatial relationship with earthquake damage in the Gölbaşı (Adıyaman) Basin using an integrated microgravity and SPAC approach. Microgravity measurements clearly delineate a deep, laterally heterogeneous basin filled with low-density alluvial and lacustrine sediments reaching thicknesses of up to approximately 700 m. The basin geometry is asymmetric and strongly controlled by strike-slip faulting associated with the East Anatolian Fault Zone. SPAC-derived shear-wave velocity profiles indicate low Vs30 values across the basin; however, spatial variations in earthquake damage cannot be explained by Vs30 alone. Quite high Vs30-based empirical estimated $Z_{1.0}$ and $Z_{2.5}$ values suggest that impedance contrasts extend to significant depths, highlighting the importance of deep basin effects. The spatial correspondence between maximum sediment thickness, deep basin parameters, and observed damage concentrations, together with the statistical correlation analysis, suggests that basin geometry and associated site conditions may have been important factors contributing to the spatial distribution of damage during the 6 February 2023 Mw 7.8 and Mw 7.6 earthquake sequence. The results suggest that one-dimensional site response models based solely on shallow soil parameters may not adequately characterize site conditions in tectonically controlled sedimentary basins. Incorporating basin geometry, lateral heterogeneity and basin-controlled site conditions may improve the assessment of seismic demand. The integration of microgravity and SPAC methods offers an efficient and practical framework for characterizing deep subsurface conditions relevant to earthquake engineering applications, particularly in urban areas where invasive investigations are limited. Overall, the findings emphasize that basin-scale effects should be considered as an important component of seismic hazard assessment in tectonically active regions. Incorporating deep basin geometry into seismic microzonation and urban planning has the potential to improve the characterization of site conditions, support more reliable ground-motion assessments, and contribute to earthquake-resilience planning for communities living in tectonically controlled sedimentary basins.

Supplementary Information The online version contains supplementary material available at https://doi.org/10.1038/s41598-026-74086-2.

Acknowledgements The authors sincerely thank the Editor and the anonymous reviewers for their constructive comments and valuable suggestions, which have greatly improved the quality of this manuscript.

Author contributions Conceptualization: A.B., Ö.B.Methodology: A.B., S.F., E.I.Software: Ö.B., E.P., N.S.I.Validation: A.B., E.I.Formal analysis: K.Ö.Ç., A.B.,Ö.B.Investigation: A.B., Ö.B., E.P.Writing—original draft preparation: A.B., Ö.B., K.Ö.Ç.Writing—review and editing: S.F., E.I., N.S.I.Visualization: K.Ö.Ç., A.B.,E.I.Supervision: E.I., A.B.,Ö.B., K.Ö.Ç.

Data availability The datasets used and/or analyzed during the current study are available from the corresponding author on reasonable request.

Declarations

Competing interests The authors declare no competing interests.

Open Access This article is licensed under a Creative Commons Attribution 4.0 International License, which permits use, sharing, adaptation, distribution and reproduction in any medium or format, as long as you give appropriate credit to the original author(s) and the source, provide a link to the Creative Commons licence, and indicate if changes were made. The images or other third party material in this article are included in the article's Creative Commons licence, unless indicated otherwise in a credit line to the material. If material is not included in the article's Creative Commons licence and your intended use is not permitted by statutory regulation or exceeds the permitted use, you will need to obtain permission directly from the copyright holder. To view a copy of this licence, visit http://creativecommons.org/licenses/by/4.0/.

References

1. Bard, P. Y. & Bouchon, M. The two-dimensional resonance of sediment-filled valleys. *Bull. Seismol. Soc. Am.* **75**(2), 519–541. https://doi.org/10.1785/BSSA0750020519 (1985).
2. Borcherdt, R. D. Estimates of Site-Dependent Response Spectra for Design (Methodology and Justification). *Earthq. Spectra*. **10** (4), 617–653 (1994).
3. Dobry, R. et al. New Site Coefficients and Site Classification System Used in Recent Building Seismic Code Provisions. *Earthq. Spectra*. **16** (1), 41–67 (2000).
4. Field, E. H. A modified ground-motion attenuation relationship for Southern California that accounts for detailed site classification and a basin-depth effect. *Bull. Seismol. Soc. Am.* **90**(6), S209–S221. https://doi.org/10.1785/0120000507 (2000).
5. Campbell, W. & Bozorgnia, Y. NGA-West2 Ground Motion Model for the Average Horizontal Components of PGA, PGV, and 5% Damped Linear Acceleration Response Spectra. *Earthq. Spectra*. **30** (3), 1087–11151. https://doi.org/10.1193/062913EQS175M (2014).
6. Wald, D. J. & Allen, T. I. Topographic slope as a proxy for seismic site conditions and amplification. *Bull. Seismol. Soc. Am.* **97**(5), 1379–1395. https://doi.org/10.1785/0120060267 (2007).
7. Castellaro, S., Mulargia, F. & Rossi, P. L. Vs30: Proxy for seismic amplification?. *Seismol. Res. Lett.* **79**(4), 540–543. https://doi.org/10.1785/gssrl.79.4.540 (2008).
8. Graves, R. W., Pitarka, A. & Somerville, P. G. Ground motion amplification in the Santa Monica area: Effects of shallow basin structure. *Bull. Seism Soc. Am.* **88**, 1224–1242 (1998).
9. Kawase, H. The Cause of the Damage Belt in Kobe: The Basin-Edge Effect, Constructive Interference of the Direct S-Wave with the Basin-Induced Diffracted/Rayleigh Waves. *Seismol. Res. Lett.* **67** (5), 25–34. https://doi.org/10.1785/gssrl.67.5.25 (1996).
10. Olsen, K. B. Site Amplification in the Los Angeles Basin from Three-Dimensional Modeling of Ground Motion. *Bull. Seismol. Soc. Am.* **90** (6), 77–94. https://doi.org/10.1785/0120000506 (2000).
11. Chiou, B. J. & Youngs, R. R. *NGA Model for Average Horizontal Component of Peak Ground Motion and Response Spectra, PEER Report 2008-09* p. 3–53 (Pacific Earthquake Engineering Research Center, University of California, 2008).
12. Chavez-Garcia, F. J. Site effects in Parkway Basin: comparison between observations and 3-D modelling. *Geophys. J. Int.* **154**, 633–646. https://doi.org/10.1046/j.1365-246X.2003.02055.x (2003).
13. Büyüksaraç, A., Işık, E. & Bektaş, Ö. A Comparative Evaluation of Earthquake Code Change on Seismic Parameter and Structural Analysis; A case of Turkey. *Arab. J. Sci. Eng.* **47**, 12301–12321. https://doi.org/10.1007/s13369-022-07099-4 (2022).
14. Goto, H., Sawada, S., Morikawa, H., Kiku, H. & Ozalaybey, S. Modeling of 3D Subsurface Structure and Numerical Simulation of Strong Ground Motion in the Adapazari Basin during the 1999 Kocaeli Earthquake, Turkey. *Bull. Seismol. Soc. Am.* **95** (6), 2197–2215. https://doi.org/10.1785/0120050002 (2005).
15. Komazawa, M. et al. Bedrock structure in Adapazarı, Turkey: a possible cause of severe damage by the 1999 Kocaeli earthquake. *Soil. Dyn. Earthq. Eng.* **22**, 829–836. https://doi.org/10.1016/s0267-7261(02)00105-7 (2002).
16. Özalaybey, S., Zor, E., Ergintav, S. & Tapırdamaz, M. C. Investigation of 3-D basin structures in the Izmit Bay area (Turkey) by single-station microtremor and gravimetric methods. *Geophy J. Int.* **186**, 883–894. https://doi.org/10.1111/j.1365-246X.2011.05085.x (2011).
17. Özel, O. & Sasatani, T. A site effect study of the Adapazari basin, Turkey, from strong- and weak-motion data. *J. Seismol.* **8**, 559–572. https://doi.org/10.1007/s10950-004-3328-8 (2004).
18. Pamuk, E., Akgün, M., Ozdağ, O. C. & Gönenç, T. 2D soil and engineering-seismic bedrock modeling of eastern part of Izmir inner Bay/Turkey. *J. App Geophy*. **137**, 104–117. https://doi.org/10.1016/j.jappgeo.2016.12.016 (2017).
19. Skrame, K. & Di Filippo, M. The Use of Gravity Prospecting to Help the Seismic Microzonation Studies of the Leonessa Basin in Rieti, Italy. *Eur. Association Geoscientists Eng. 7th Congress Balkan Geophys. Soc.* cp–362. https://doi.org/10.3997/2214-4609.20131829 (2013).
20. El Hilali, M., Bounab, A., Timoulali, Y., El Messari, J. E. S. & Ahniche, M. Seismic site-effects assessment in a fluvial sedimentary environment: Case of Oued Martil floodplain, Northern Morocco. *Nat. Hazards* **118**, 1235–1257. https://doi.org/10.1007/s11069-023-06032-8 (2023).
21. Mohamed, E. H., Ouahabi, A. T. & Mohamed, A. Seismic Site-Effect Characterization of the High Atlas Sedimentary Basin Following the 2023 Al Haouz Earthquake. In: Ilki, A., Goksu, C., Cinar, T., Erdik, M. (eds) Proceedings of the 10th Turkish Conference on Earthquake Engineering. TCEE 2025. Lecture Notes in Civil Engineering, 843. Springer, Cham. (2026). https://doi.org/10.1007/978-3-032-20881-1_22
22. Emre, Ö. et al. *Active fault map of Turkey with an explanatory text 1:1,250,000 scale* (General Directorate of Mineral Research and Exploration, 2013). Special Publication Series 30.
23. Barka, A. A. The North Anatolian Fault Zone. *Ann. Tectonicae*. **6** (Special Issue), 164–195 (1992).

24. Büyüksaraç, A., Işık, E., Bektaş, O. & Avcil, F. Achieving intensity distributions of 6 February 2023 Kahramanmaraş (Türkiye) earthquakes from peak ground acceleration records. *Sustainability* **16**, 599. https://doi.org/10.3390/su16020599 (2024a).
25. Özden, S., Gündogdu, E. & Bekler, T. Interactions between Eurasian/African and Arabian plates: Eskişehir Fault, NW Turkey. *J. Afr. Earth Sci.* **111**, 349–362. https://doi.org/10.1016/j.jafrearsci.2015.08.014 (2015).
26. Şengör, A. M. C. The North Anatolian transform fault: its age, offset and tectonic significance. *J. Geol. Soc. Lond.* **136**, 269–282. https://doi.org/10.1144/gsjgs.136.3 (1979).
27. İmamoğlu, M. Ş. *Gölbaşı (Adıyaman)-Pazarcık-Narlı(K.Maraş) Arasındaki Sahada Doğu Anadolu Fayı'nın Neotektonik İncelemesi* 159 (Ankara Üniversitesi Fen Bilimleri Enstitüsü, 1993). unpublished thesis.
28. Çoğurcu, M. T. Construction and design defects in the residential buildings and observed earthquake damage types in Turkey. *Nat. Hazards Earth Syst. Sci.* **15**, 931–945 (2015).
29. Dimova, S. L. & Negro, P. Influence of construction deficiencies on the seismic response of structures. *Earthq. Eng. Struct. Dyn.* **34**, 613–635. https://doi.org/10.1002/eqe.436 (2005).
30. Isık, E. et al. Failures in Reinforced-Concrete Columns and Proposals for Reinforcement Solutions: Insights from the 2023 Kahramanmaraş Earthquakes. *Buildings* **15**, 1535. https://doi.org/10.3390/buildings15091535 (2025a).
31. Isık, E., Avcil, F., Büyüksaraç, A. & Arkan, E. Comparative Analysis of Target Displacements in RC Buildings for 2023 Türkiye Earthquakes. *Appl. Sci.* **15**, 4014. https://doi.org/10.3390/app15074014 (2025b).
32. Akar, F. et al. Geotechnical and structural damages caused by the 2023 Kahramanmaraş earthquakes in Gölbaşı (Adıyaman). *Appl. Sci.* **14**, 2165. https://doi.org/10.3390/app14052165 (2024).
33. Ecemiş, N., Donmez, C., Karaman, M., Valizadeh, H. & Dalgic, K. D. Assessment of seismic liquefaction and structural instability in Adıyaman-Gölbaşı after the February 6, 2023, earthquakes in Türkiye. *Soil. Dyn. Earthq. Eng.* **192**, 109300. https://doi.org/10.1016/j.soildyn.2025.109300 (2025).
34. Pulsoni, M., Chiaradonna, A., Sezer, A. & Monaco, P. Liquefaction-induced damage assessment in Golbasi city after the 6th of February 2023 Türkiye earthquakes. *JGS Special Publication*. **10** (50), 1889–1894. https://doi.org/10.3208/jgssp.v10.OS-39-06 (2024).
35. Ünal, H. & Ergüler, Z. A. Kahramanmaraş Depremlerinin Adıyaman-Gölbaşı Yerleşim Alanındaki Mühendislik Yapılarına Etkisi ve Deprem-Zemin Etkileşimi. *Yerbilimleri* **44**(3), 202–221. https://doi.org/10.17824/yerbilimleri.1313819 (2023).
36. Tonuk, G. et al. Geotechnical damages observed in the 2023 Turkey-Syria Earthquake. *JGS Special Publication*. **10** (44), 1659–1664. https://doi.org/10.3208/jgssp.v10.OS-33-05 (2024).
37. Çetin, K. O., Soylemez, B., Guzel, H. & Cakir, E. Soil liquefaction sites following the February 6, 2023, Kahramanmaraş-Türkiye earthquake sequence. *Bull. Earthq. Eng.* **23**(3), 921–944. https://doi.org/10.1007/s10518-024-01875-3 (2025b).
38. Demir, A. et al. Destructive impact of successive high magnitude earthquakes occurred in Türkiye's Kahramanmaraş on February 6, 2023. *Bull. Earthq. Eng.* **23**(3), 893–919. https://doi.org/10.1007/s10518-024-01865-5 (2025).
39. Flora, A. et al. Liquefaction effects in the city of Gölbaşı: from the analysis of predisposing factors to damage survey. *Eng. Geol.* **338**, 107633. https://doi.org/10.1016/j.enggeo.2024.107633 (2024).
40. Taftsoglou, M., Valkaniotis, S., Papathanassiou, G. & Karantanellis, E. Satellite imagery for rapid detection of liquefaction surface manifestations: The case study of Türkiye–Syria 2023 earthquakes. *Remote Sens.* **5**(17), 14190. https://doi.org/10.3390/rs15174190 (2023).
41. Moug, D., Bray, J., Bassal, P., Kendir, S. B. & Sahin, A. Lidar Scans of Geotechnical Earthquake Damage at Building Sites in Gölbaşı, Adıyaman. in *GEER* Lidar Data from the 2023 Kahramanmaras Earthquake Sequence Reconnaissance [Version 2]. DesignSafe-CI. (2024). https://doi.org/10.17603/ds2-fcry-0191
42. Zeybek, A., Yıldız, Ö. & Sönmezer, Y. B. Post-earthquake assessment of liquefaction in Gölbaşı-Adıyaman following the 6 February 2023 Kahramanmaraş earthquakes: Field observations, SPT-based analysis, and laboratory testing of soil ejecta. *Nat. Hazards* **121**(20), 24157–24206. https://doi.org/10.1007/s11069-025-07715-0 (2025).
43. Çetin, K. O. et al. Ground failures and foundation performances in Adıyaman–Gölbaşı following the 6 February 2023 Kahramanmaraş–Türkiye earthquake sequence. *Earthq. Spectra*. **41** (1), 249–289. https://doi.org/10.1177/87552930241270581 (2025).
44. Öser, C. et al. Geotechnical aspects and site investigations on Kahramanmaraş earthquakes, February 06, 2023. *Nat. Haz.* **121** (5), 5637–5668. https://doi.org/10.1007/s11069-024-07028-8 (2025).
45. Provost, F. et al. High-resolution co-seismic fault offsets of the 2023 Türkiye earthquake ruptures using satellite imagery. *Sci. Rep.* **14**(1), 6834. https://doi.org/10.1038/s41598-024-55009-5 (2024).
46. Toprak, S. et al. Assessment of Infrastructure Failures in the 2023 Kahramanmaraş Earthquakes. *ASCE OPEN.* **4** (1), 04026001. https://doi.org/10.1061/AOMJAH.AOENG-0103 (2026).
47. Akkaya, İ., Özvan, A., Tapan, M. & Şengül, M. A. Determining the site effects of 23 October 2011 earthquake (Van province, Turkey) on the rural areas using HVSR microtremor method. *J. Earth Syst. Sci.* **124**, 1429–1443. https://doi.org/10.1007/s12040-015-0626-1 (2015).
48. Asten, M. W., Askan, A., Ekincioglu, E. E., Sisman, F. N. & Ugurhan, B. Site characterisation in north-western Turkey based on SPAC and HVSR analysis of microtremor noise. *Explor. Geophys.* **45**(2), 74–85 (2014).

49. Gök, E. & Polat, O. Microtremor HVSR study of site effects in Bursa city (Northern Marmara Region, Turkey). In the Book of Earthquake Research and Analysis - New frontiers in Seismology (Ed., Sebastiano d'Amico, 380 p.), INTECH Publications, University Campus, Rijeka - Croatia, ISBN 978-953-307-840-3, 225–236. (2012).
50. Pamuk, E. et al. Three-dimensional shear wave velocity (Vs) structure and dynamic soil properties of Adıyaman-Gölbaşı basin using HVSR and SPAC methods. *Soil. Dyn. Earthq. Eng.* **200**, 109744. https://doi.org/10.1016/j.soildyn.2025.109744 (2026).
51. Nettletton, L. I. *Geophysical Prospecting for Oil* 452 (McGraw Hill Book Company, Inc., 1940).
52. Vening Meinesz, F. A. Gravity and the hypothesis of convection currents in the earth. *Proc. Kon Ned Akad. Wetensch*. **37**, 37–45 (1934).
53. Çıplak, R. & Akyüz, H. S. Gölbasi Pull-Apart Basin on the East Anatolian Fault Zone, Turkey. *GSA Annual Meeting Denver Geol. Soc. Am. Abstracts*. **36** (5), 148 (2004).
54. Yönlü, Ö., Altunel, E., Karabacak, V. & Akyüz, H. S. Evolution of the Gölbas¸ ı basin and its implications for the long-term offset on the East Anatolian Fault Zone, Turkey. *J. Geodyn.* **65**, 72–281. https://doi.org/10.1016/j.jog.2012.04.013 (2013).
55. Mann, P., Hempton, M. R., Bradley, D. C. & Burke, K. Development of Pull-Apart Basins. *J. Geol.* **91**, 529–554 (1983).
56. Smit, J., Brun, J. P., Cloetingh, S. & Ben-Avraham, Z. Pull-apart basin formation and development in narrow transform zones with application to the Dead Sea Basin. *Tectonics* **27**, TC6018. https://doi.org/10.1029/2007TC002119 (2008).
57. Semblat, J. F. et al. Seismic wave amplification: Basin geometry vs soil layering. *Soil Dyn. Earthq. Eng.* **25**(7–10), 529–538. https://doi.org/10.1016/j.soildyn.2004.11.003 (2005).
58. Sreejaya, K. P., Behera, S. N. & Raghukanth, S. T. G. Effect of basin geometry in seismic wave amplification. *J. Earth Syst. Sci.* **134**, 166. https://doi.org/10.1007/s12040-025-02616-z (2025).
59. Gupta, S. V., Parvez, I. A. & Khan, P. K. Imaging subsurface geological complexity (2D/3D) beneath the Greater Srinagar region of the Kashmir Basin, Northwest Himalaya. *Near Surf. Geophys.* **20**, 94–114. https://doi.org/10.1002/nsg.12186 (2022a).
60. Gupta, S. V., Parvez, I. A. & Khan, P. K. Site response analysis beneath the Kashmir basin (NW Himalaya) using ambient noise. *Earthq. Spectra* **39**, 2436–2469. https://doi.org/10.1177/87552930231195640 (2023).
61. Gupta, S. V., Parvez, I. A., Ankit Khan, P. K. & Chandra, R. Site Effects Investigation in Srinagar City of Kashmir Basin Using Microtremor and Its Inversion. *J. Earthq. Eng.* **26** (7), 3799–3820. https://doi.org/10.1080/13632469.2020.1816232 (2022b).
62. Büyüksaraç, A., Gündoğdu, E., Bektaş, Ö. & Işık, E. Failure mechanism by wrench faulting in Central Anatolia. *Eng. Fail. Anal.* **156**, 107786. https://doi.org/10.1016/j.engfailanal.2023 (2024b).

Publisher's note Springer Nature remains neutral with regard to jurisdictional claims in published maps and institutional affiliations.

Authors and Affiliations

Aydın Büyüksaraç[1] · Özcan Bektaş[2] · Eren Pamuk[3] · Seyhan Fırat[4] · Ercan Işık[5] · Nihat Sinan Işık[4] · Kemal Önder Çetin[6]

✉ Aydın Büyüksaraç
absarac@comu.edu.tr

[1] Çan Vocational School, Çanakkale Onsekiz Mart University, Çanakkale TR-17400, Türkiye

[2] Department of Geophysical Engineering, Sivas Cumhuriyet University, Sivas, Türkiye

[3] Institute of Earthquake Technologies, Erzincan Binali Yıldırım University, Erzincan, Türkiye

[4] Department of Civil Engineering, Faculty of Technology, Gazi University, Ankara, Türkiye

[5] Department of Civil Engineering, Faculty of Engineering and Architecture, Bitlis Eren University, Bitlis TR-13000, Türkiye

[6] Department of Civil Engineering, Middle East Technical University, Ankara, Türkiye